Theoretical Studies of the Active-Site Structure, Spectroscopic and Thermodynamic Properties, and Reaction Mechanism of Multicopper Oxidases

Rulisek, Lubomir; Ryde, Ulf

Published in:
Coordination Chemistry Reviews

DOI:
10.1016/j.ccr.2012.04.019

2013

Theoretical Studies of the Active-Site Structure, Spectroscopic and Thermodynamic Properties, and Reaction Mechanism of Multicopper Oxidases

Lubomír Rulíšek, Ulf Ryde

Institute of Organic Chemistry and Biochemistry, Gilead Sciences & IOCB Research Center, Academy of Sciences of the Czech Republic, Flemingovo náměstí 2, 166 10 Prague 6, Czech Republic

Department of Theoretical Chemistry, Lund University, Chemical Centre, P. O. Box 124, SE-221 00 Lund, Sweden

Email: rulisek@uochb.cas.cz; ulf.ryde@teokem.lu.se

Tel. (Fax): +420-220-183-263(578)

Contents:

ABSTRACT. In this article, we review recent theoretical work that has complemented the extensive experimental data available for multicopper oxidases (MCO) and led to the elucidation of the reaction mechanism of this class of enzymes. The MCOs couple four one-electron oxidations of substrates at the mononuclear type 1 copper (Cu-T1) site with the four-electron reduction of dioxygen at the trinuclear copper cluster (TNC). The TNC consists of three copper ions arranged in a unique triangular fashion. In its oxidised form and in some experimentally observed intermediates (the peroxy and native intermediates), this leads to a magnetic coupling of the unpaired electrons of the three copper ions, resulting in unusual spectroscopic features. By correlating experimental and theoretical data, an unambiguous mapping between the structural, energetic and spectroscopic properties of the various intermediates in the MCO reaction cycle can be established. In terms of theory, these studies involved quantum mechanics (QM; density-functional theory and multi-reference self-consistent field) calculations, combined QM and molecular mechanics (QM/MM) modelling, ranging from standard QM/MM optimisations to the combination of QM/MM optimisation with EXAFS spectroscopy and QM/MM free-energy perturbations to accurately address phenomena such as the Cu-T1 → TNC electron transfer, as well as the reduction potentials and acid constants of all the putative intermediates in the MCO reaction cycle. In summary, we try to demonstrate in this review that the MCOs are not only an attractive playground for theoretical methods, but the results of the calculations (when carefully correlated with and benchmarked against experimental data) can also be used to draw unambiguous conclusions about MCO structure and reactivity.

1. Introduction

The multicopper oxidases (MCOs) form a class of enzymes playing a variety of physiological roles in organisms, having in common the presence of two copper sites that accommodate four copper ions in total. Utilising these specific features, the MCOs couple four one-electron oxidations of a substrate with a four-electron reduction of molecular oxygen to water [1,2]:

$$O_2 + 4e^- + 4H^+ \rightarrow 2H_2O \qquad (1).$$

This reaction takes place at a trinuclear copper cluster (TNC), whereas the substrate is oxidised at a type 1 copper site (Cu-T1), which is ~13 Å away from the TNC. The two sites are connected via a bifurcated $(Cu_{TNC}–His)_2–Cys–Cu_{T1}$ protein chain (where His–Cys–His are three consecutive residues in the protein, of which the two histidines are ligands of two copper ions in the TNC and the Cys is coordinated to the Cu-T1 ion as cysteinate, Figure 1). This structural arrangement is assumed to provide an efficient electron-transfer (ET) pathway between the two sites, transferring the four electrons that are needed for the dioxygen reduction from the Cu-T1 site to the TNC. Therefore, the oxidation states of four copper ions span the full spectrum between $(Cu^{2+})_4$ and $(Cu^+)_4$. The MCO family includes enzymes catalysing the oxidation of small organic substrates, such as plant and fungal laccases, ascorbate oxidase, bilirubin oxidase, phenoxazinone synthase, CotA protein, and highly specific enzymatic oxidants of metal ions, such as ceruloplasmin, Fet3p, CueO and MnxG) [3].

The study of the MCOs has a long history. However, judged by the number of crystallographic studies and spectroscopic findings, the experimental research has greatly intensified during the last two decades. One of the most remarkable achievements that can be attributed to a careful interpretation of the spectroscopic data is the postulation of the TNC itself (i.e. three copper ions bound at a distance of 3–5 Å) [4]. In the early 1990s, this hypothesis was confirmed by the crystal structures of ascorbate oxidase [5], showing a TNC, consisting of a pair of type 3 copper ions (Cu-T3), coordinated to three histidine groups each and in the oxidised state bridged by an oxo or hydroxide ion, and one type 2

copper ion (Cu-T2), coordinated by two histidine residues and a water molecule or hydroxide ion (Figure 1). Most of these achievements are well documented in many extensive and excellent reviews [2,6,7,8,9,10,11] on the MCO structure, reactivity and spectroscopy written over the years, which also provide a historical record of the evolution of our understanding of their complex molecular architecture.

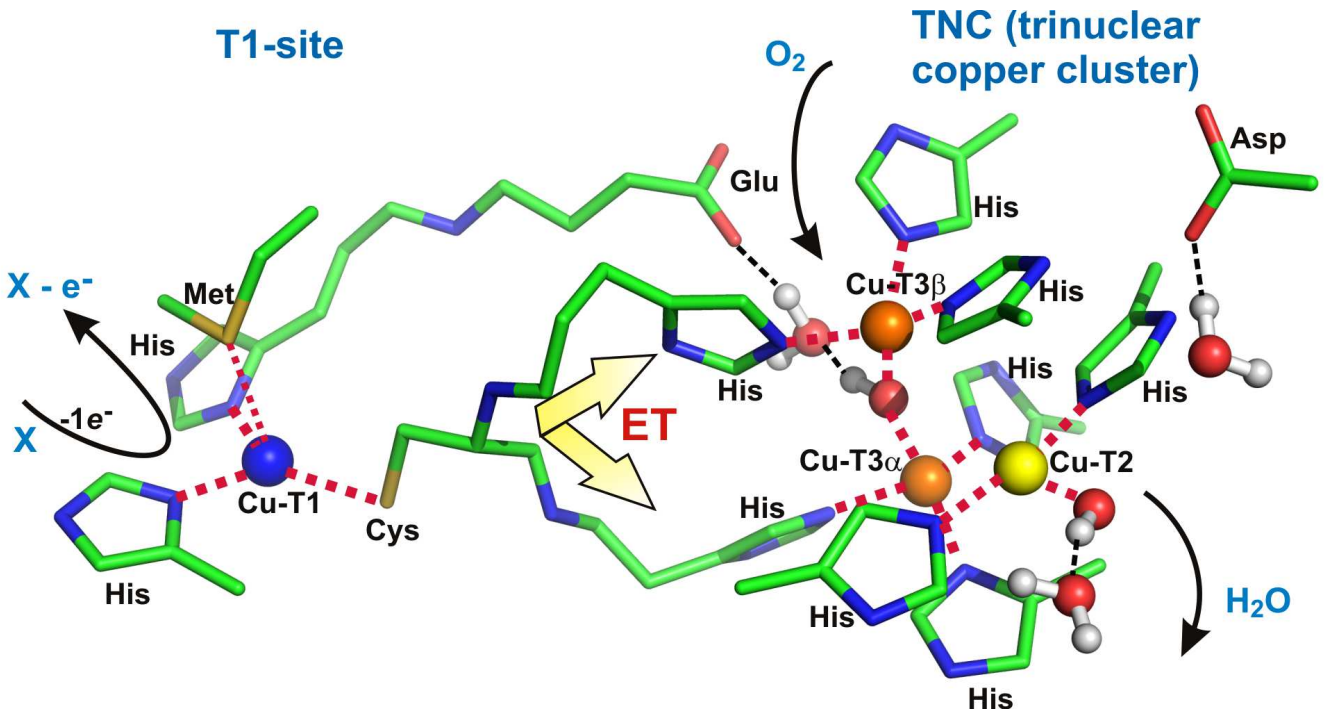

Figure 1: The general architecture of the trinuclear copper cluster site (the site of the four-electron O_2 → H_2O reduction) and of the Cu-T1 site (the site of one-electron oxidations of organic substrates or metal ions). The figure shows a QM/MM model of the resting oxidised state in the CueO enzyme (PDB code 1KV7) [12]. The likely electron-transfer pathway via the bifurcated Cys-$(His)_2$ chain is depicted together with an alternative His-X-Glu connection between the Cu-T1 and Cu-T23 sites. The coordination bonds are depicted by red dotted lines (with a thinner line used for the coordination of the Met residue in Cu-T1 site, which is not present in all MCOs). Three solvent molecules with positions obtained by QM/MM modelling are displayed as well, which can be part of water exit channel. Black dashed lines are used for hydrogen bonds.

The aim of this review is to show that the MCOs and smaller inorganic models of the TNC present a highly challenging playground for computational chemistry and demonstrate how recent theoretical contributions have assisted in our understanding of the details of the MCO reaction mechanism. It must be mentioned that this task would not have been possible without the large amount of spectroscopic data and crystal structures of MCOs available.

What makes the MCOs so interesting for a computational bioinorganic chemist? We can conceive at least three reasons. The first is the inherent (*in vacuo*) instability of many plausible intermediates in the catalytic cycle of MCOs (i.e. the geometrical arrangements of the TNC) as a consequence of the four distinct redox states of the three copper ions (i.e. $(Cu^{2+})_3$, $(Cu^{+})(Cu^{2+})_2$, $(Cu^{2+})(Cu^{+})_2$ and $(Cu^{+})_3$) coupled with the various accessible protonation states of the copper ligands originating from water or dioxygen (e.g. oxo, hydroxo and peroxo species) [13]. Therefore, the TNC site (the Cu ions with their first-sphere ligands) possesses a high positive charge (+3 or +4 according to the suggested reaction mechanism), which is partly compensated for by two carboxylate residues in the second coordination sphere of the TNC, which are conserved throughout the MCO family (Figure 1) [14]. The second reason is the complicated electronic structure of the TNC. In the putative structure of the so-called native intermediate, **NI**, the TNC contains three unpaired spins at the vertices of a triangle, all coupled via an O_2^{2-} molecule in the centre. This leads to so-called spin-frustration, which means that the exchange coupling between the three pairs of Cu^{2+} ions cannot be satisfied. In this oxidation state, there are two doublet states and one quartet state close in energy (within a few hundred cm^{-1}) [15]. The third reason is the unique opportunity to couple the theoretical calculations directly to experimental data and provide their theoretical interpretation [16].

2. Multicopper Oxidases: The Peculiar Spectroscopic and Structural Features of the Trinuclear Copper Cluster

In this section, we shortly review two important sources of experimental information that have been crucial for our understanding of the structure and function of the MCOs: the X-ray crystallographic data and spectroscopic (absorption, circular dichroism – CD, magnetic circular dichroism – MCD, electron paramagnetic resonance – EPR, X-ray absorption spectroscopy – XAS, and extended X-ray absorption fine structure – EXAFS) findings. Whereas the former is an essential prerequisite for theoretical studies, particularly for modelling with combined quantum mechanics and molecular mechanics (QM/MM) methods, the latter information assists in accepting or rejecting potential structural candidates for the intermediates in the reaction cycle of the studied enzyme. This is of utmost importance, since theoretical calculations mostly complement experimental data by providing an energy characterisation of the species involved. However, this energy mapping (albeit indispensable) has two drawbacks: the inherent errors of the method used and the fact that reaction pathways that differ in the number of protons and electrons cannot be directly compared, or more precisely, become comparable only after connecting them via calculated reduction potentials and acidity constants (pK_as), which are difficult to estimate with a high accuracy. Therefore, the theoretical modelling of bioinorganic species will, to a great extent, rely heavily upon accurate structural and spectroscopic data.

2.1. MCO Crystal Structures: The Problem of Partially Reduced Copper Ions

The first crystal structures of a MCO (ascorbate oxidase) containing a full complement of copper ions were published 1992 by Messerschmidt et al. [5]. Ten years later, these were followed by the first structures of laccases [17,18] and CueO [12]. In December 2011, there were more than fifty crystal structures of MCOs in the Protein Data Bank (PDB). The structures with a resolution better than 2.0 Å are compiled in Table 1 along with selected interatomic distances within the TNC cluster.

Table 1. A summary of three-dimensional crystal structures of MCOs containing a full complement of copper ions with a resolution higher than 2.0 Å (out of 53 structures in total) deposited in the Protein Data Bank in December 2011. All distances are in Å. The distances r_{23}, $r_{23'}$ and $r_{33'}$ are between the three copper ions, the r_{2L} distance is between Cu-T2 and its coordinated solvent molecule, whereas r_{3B} and $r_{3'B}$ are the distances between the two Cu-T3 ions (Cu3 and Cu3') and the bridging molecule (solvent, peroxide, O_2, N_3^-, or Cl^-). $\alpha_{3B3'}$ is the angle between Cu3, the bridging ligand (if present) and Cu3'. N.r. indicates that the redox state was not reported in publication accompanying the structure.

PDB code	Resol [Å]	Redox State	Enzyme	Source	r_{23} [Å]	$r_{23'}$ [Å]	$r_{33'}$ [Å]	r_{2L} [Å]	r_{3B}; $r_{3'B}$ [Å]	$\alpha_{3B3'}$ [deg]	Ref	Comments
2HRG	1.58	*n.r.*	Laccase	*Trametes trogii*	4.1	4.5	5.2	2.6	3.0;2.2	170	-	
2QT6 (subunit A)	1.50	Partially reduced	Laccase	*Lentinus tigrinus*	4.1	4.3	4.9	2.4	3.0;2.2	149	[19]	oxygen atom in the centre of the TNC (μ-3-oxo coordination)
2QT6 (subunit B)	1.50	Partially reduced	Laccase	*Lentinus tigrinus*	4.1	4.3	4.9	2.5	-	-	[19]	O_2 between Cu3-Cu3' d(O-O) = 1.5 Å
2Q9O	1.30	Partially reduced	Laccase	*Melanocarpus albomyces*	4.0	4.0	4.7	2.5	-	-	[20]	Cu-T2 ligand is a Cl^- ion; O_2 with d(O-O) = 1.1 Å symmetrically bound between Cu3/3'
3FPX	1.80	*n.r.*	Laccase	*Trametes hirsuta*	3.8	4.1	3.8	2.1	2.4;1.7	132	-	oxygen atom in the centre of the TNC (μ-3-oxo coordination)
3DIV	1.76	*n.r.*	Laccase	*Cerrana maxima*	4.0	4.4	4.8		2.5;2.3	176	-	
3FU7	1.67	Partially reduced	Laccase	*Melanocarpus albomyces*	4.1	4.1	5.0	2.8	-	-	[21]	Cu-T2 ligand is a Cl^- ion; O_2 with d(O-O) = 1.1 Å symmetrically bound between Cu3/3'; soaked with 2,6-dimethoxyphenol
3GDC	1.80	*n.r.*	MCO	*Arthrobacter sp.*	4.0	4.3	5.6	3.3	2.9;2.7	177	-	In subunit A of the trimer
2WSD	1.60	Partially reduced	CotA laccase	*Bacillus subtilis*	3.6	4.0	4.8	3.0	-	-	[22]	O_2; d(O-O) = 0.8 Å symmetrically bound between Cu3/3'
3G5W	1.90	Partially reduced	MCO	*Nitrosomonas europaea*	4.0	4.1	5.0	2.8	2.7;2.4	170	[23]	In subunit A of the hexamer
3ZX1	1.95	Partially reduced	Metallo-oxidase	*Campylobacter jejuni*	3.6	3.6	4.4	3.2	-	-	[24]	O_2; d(O-O) = 1.2 Å symmetrically bound between Cu3/3'; partial depletion of Cu-T2
1W6L	2.00	Partially	Cot A laccase	*Bacillus subtilis*	3.7	4.0	4.7	3.0	-	-	[11]	O_2; d(O-O) = 1.2 Å symmetrically bound between Cu3/3'

		reduced										
2X88	1.80	Partially reduced	Cot A laccase	*Bacillus subtilis*	3.8	4.1	4.8	2.9	-	-	[25]	O_2; d(O-O) = 1.2 Å symmetrically bound between Cu3/3'
2ZWN	1.70	*n.r.*	Recombinant laccase (mgLAC)	Metagenomes	3.9	4.1	4.9	3.0	2.6;2.4	177	[26]	
2FQE	1.92	*n.r.*	CueO	*Escherichia coli*	3.4	3.9	4.2	3.0	2.1;2.1	179	[27]	
3QPK	1.90	Partially reduced?	Laccase	*Melanocarpus albomyces*	4.0	4.0	5.0	2.9	2.6;2.4	179	[28]	The enzyme pressurised with xenon, distances in subunit A
4A2E	1.80	*n.r.*	Laccase	*Coriolopsis gallica*	4.0	4.4	5.0	2.8	2.7;2.3	172	-	
2XYB	1.75	Partially reduced	Laccase	*Pycnoporus cinnabarinus*	4.0	4.1	4.7	2.8	-	-	-	O_2 moiety (peroxide?) with d(O-O) = 1.4 Å bound between Cu3/3' in Cu_2 η1: η1 O_2 coord. mode
1V10	1.70	Partially reduced	Laccase	*Rigidosporus lignosus*	4.0	4.1	5.1	2.4	3.4;2.1	162	[29]	
2H5U	1.90	*n.r.*	Laccase	*Cerrena maxima*	4.1	4.4	4.8	2.6	3.0;1.8	171	[30]	
2XU9	1.50	*n.r.*	Laccase	*Thermus thermophilus* Hb27	3.7	3.9	5.0	2.2	2.5;2.5	173	-	OH^- (1.1 Å) bound in between Cu3/3'
1GYC	1.9	Oxidised	Laccase	*Trametes versicolor*	3.8	3.8	3.9	2.4	2.1;2.2	152	[17]	
1KYA	2.4	Oxidised	Laccase with 2,5-xylidine	*Trametes versicolor*	3.9	3.9	3.9	2.4	1.9;2.1	162	[31]	
1AOZ	1.9	Oxidised	Ascorbate oxidase	Zucchini	3.8	3.8	3.7	2.0	2.0;2.0	135	[5]	
1GSK	1.7	Partially reduced	CotA	*Bacillus subtilis*	4.6	4.7	4.3	2.1	2.1;2.2	168	[32]	Cu-T2 trigonal
1KV7	1.4	Partially reduced	CueO	*Escherichia coli*	3.5	4.0	4.7	3.0	2.3;2.4	170	[12]	
1N68	1.7	Partially reduced	CueO with regulatory Cu ion	*Escherichia coli*	3.6	4.1	4.8	2.9	2.3;2.5	176	[33]	
1PF3	1.5	Partially reduced	CueO M441L mutant	*Escherichia coli*	3.8	4.2	4.8	2.8	2.4;2.5	171	[33]	

As can be seen from Table 1, the general constitution of the TNC is very similar over the range of the MCOs compiled in the table. From a theoretical point of view, the important issue is the sensitivity of the interatomic Cu–Cu and Cu–O distances to the oxidation states of the TNC and protonation states of the oxy-, hydroxy-, O_2^{n-}, or water ligands. The Cu–Cu distances range between 3.5 and 5.6 Å (Table 1) and the Cu3–Cu3' distance is usually longest. As also reflected in QM/MM calculations (cf. Section 3.1), the longer Cu-Cu distances are generally found in the structures containing the reduced copper ions. In the third column of Table 1, we have tried to conjecture the oxidation state of the TNC from the information available in the corresponding papers cited in column 12, to which the reader is referred for further information. It was often difficult to make such an assignment and many structures most likely represent time averages of structures with varying oxidation states of copper ions in the TNC, because the crystals suffer from radiation damage and reduction upon irradiation by X-rays [20] (this is denoted "partially reduced" in Table 1). While this does not really present a stumbling block for the theoretical modelling, it limits the direct comparison of various intermediates with the X-ray crystallographic data. This is also related to ongoing discussions on the nature of the bridging ligand. As can be seen in Table 1, a dioxygen ligand is present in some of the crystal structures [11, 19, 20, 21, 22, 24, 25] and its presence is also supported by paramagnetic NMR studies [34]. Since inorganic experience, spectroscopic data, and computational studies tell us that O_2 binds only to Cu^+ [8,9,10,13], this indicates that such structures are reduced during data collection.

In spite of these drawbacks, the crystal structures are essential for the QM/MM modelling of the reaction mechanism. Moreover, they provide an invaluable source of information of structurally conserved motifs in the MCOs, e.g. the four His–X–His motifs binding three Cu ions in the TNC, two water molecules in the vicinity of Cu-T2 ligand, one water molecule hydrogen-binding to the Cu-T3 bridging ligand, one carboxylate group ~6 Å from the Cu-T3 ions, another carboxylate group ~6 Å from the Cu-T2 ion (Figure 1), and the dioxygen entrance channel that has been probed by xenon by Kalio et al. [28].

2.2. A Brief Overview of the Spectroscopic Findings. The enormous amount of spectroscopic information on the MCOs has been extensively described in many of the reviews mentioned above; for a recent summary we recommend Ref. [10]. In this short paragraph, we will only extract the spectroscopic data that can be correlated to computations. A major outcome of the experiments was the spectroscopic definition of two intermediates – the peroxy intermediate, **PI** [35], and the **NI** [15], in which the dioxygen is $2e^-$ reduced and fully ($4e^-$) reduced, respectively. Based on kinetic studies, the conversion of the **NI** into the resting oxidised state (**Ox**) is slow, and therefore **NI** seems to be the only catalytically relevant fully oxidised form of the enzyme and as such, it is in turn presumably directly reduced into the fully reduced form (**Red**) of the enzyme. However, to the best of our knowledge, conclusive and comprehensive evidence concerning the order of protonations, reductions (ET from Cu-T1) and dehydrations of the **NI** to reach the **Red** state has not yet been published. The same holds true for the full **Ox** → **Red** pathway, whereas the slow **NI** → **Ox** pathway is discussed in Ref. [36]. It should be noted that alternative mechanisms, with O_2 binding to the fully oxidised state, have also been suggested, based on crystal structures [11]. However, such a mechanism has been hard to reconcile with available inorganic, kinetic, and computational data [8,9,10,13] and it does not take into account the fact that crystal structures are photoreduced during data collection.

The Cu-T1 site has a strong absorption band around 600 nm, arising from a $S_{Cys} \rightarrow Cu^{II}$ charge-transfer (CT) excitation, which gives rise to the intense blue colour of the MCOs [2]. Similar Cu-T1 sites are encountered in blue-copper proteins, the spectra of which have been theoretically investigated by many researchers (for an example see Refs. [37,38]). Of greater interest for this review is the Cu-T3 antiferromagnetically coupled pair that exhibits a characteristic 330-nm absorption band arising from an $OH^- \rightarrow Cu^{II}$ charge-transfer transition in the **Ox** state [39]. Large amounts of spectroscopic information are also available for the **NI** [15]. As briefly mentioned above, it has a doublet ground state with a thermally populated excited doublet state at ~150 cm^{-1} and the first quartet at ~520 cm^{-1}. Spin-frustration of the TNC gives rise to a broad EPR signal with two of the *g* values below 2, which is quite unusual for copper. The XAS Cu K-edge spectrum shows that the TNC is fully oxidised and it exhibits two charge-

transfer transitions at 365 and 318 nm. From the EXAFS data, it was concluded that there are two or three short Cu–Cu distances of ~3.3 Å. One of the most convincing experimental proofs of the **NI** structure was provided by an analysis of the MCD spectrum (the so-called pseudo A-term) [40] and its comparison with inorganic model complexes.

The **PI** is the likely precursor of the **NI** in the catalytic cycle and it has been prepared by removal of the Cu-T1 ion and its replacement with a Hg^{2+} ion [35]. SQUID magnetic susceptibility studies have led to the assignment of an antiferromagnetically coupled singlet ground state, with the Cu-T2 ion and one of the Cu-T3 ions oxidised, while the second Cu-T3 ion is reduced. This has been confirmed in a recent mutation study of the Fet3p protein, in which the histidines binding the TNC copper ions were replaced with glutamines and it was shown that there exists an asymmetry between the two T3 copper ions in a sense that the loss of the His ligand for one of them turns off the O_2 reactivity [41]. The EXAFS spectrum of the **PI** indicates that there is one short Cu–Cu distance of ~3.4 Å.

Finally, a related state has also been studied spectroscopically, viz. the peroxy adduct (**PA**), which is a catalytically non-relevant, reasonably stable peroxide adduct of the **Ox** state of the enzyme (which lacks two electrons that are necessary for the reduction of the peroxide, compared to the **PI**) [42]. The **PA** has been shown to share many spectroscopic features with the **PI**, e.g. the Cu–Cu distances determined by EXAFS and the antiferromagnetic coupling of two copper ions (with one extra spin on the third copper).

With all this spectroscopic information at hand, one may start to formulate a plausible reaction mechanism for the MCOs and attempt to fill in the missing pieces of the overall mosaic by means of theoretical calculations.

3. Theoretical Calculations of the MCO Intermediates

3.1. Structural and Energetic Characterisation of Key Intermediates in the MCO Reaction Cycle by Theoretical Calculations. The spectroscopic findings led to the suggestion of two structural

candidates each for the **PI** and **NI**, shown Figure 2, [15,35]. To resolve this ambiguity and also to study the other key states in the reaction mechanism, **Ox**, **Red**, as well as a one-electron reduced form of the **PI**, called **NI'** in the following, an exhaustive QM/MM investigation of the TNC making use of the best crystal structure of a MCO available at that time, CueO, was performed [13]. The quantum mechanical calculations were performed at the at the density functional theory (DFT) level. The geometric and energetic data provided significant insight into the experimentally observed intermediates and allowed us for the first time to suggest a reasonable reaction cycle for O_2 reduction, as shown in Figure 3, thus nicely complementing the extensive experimental data.

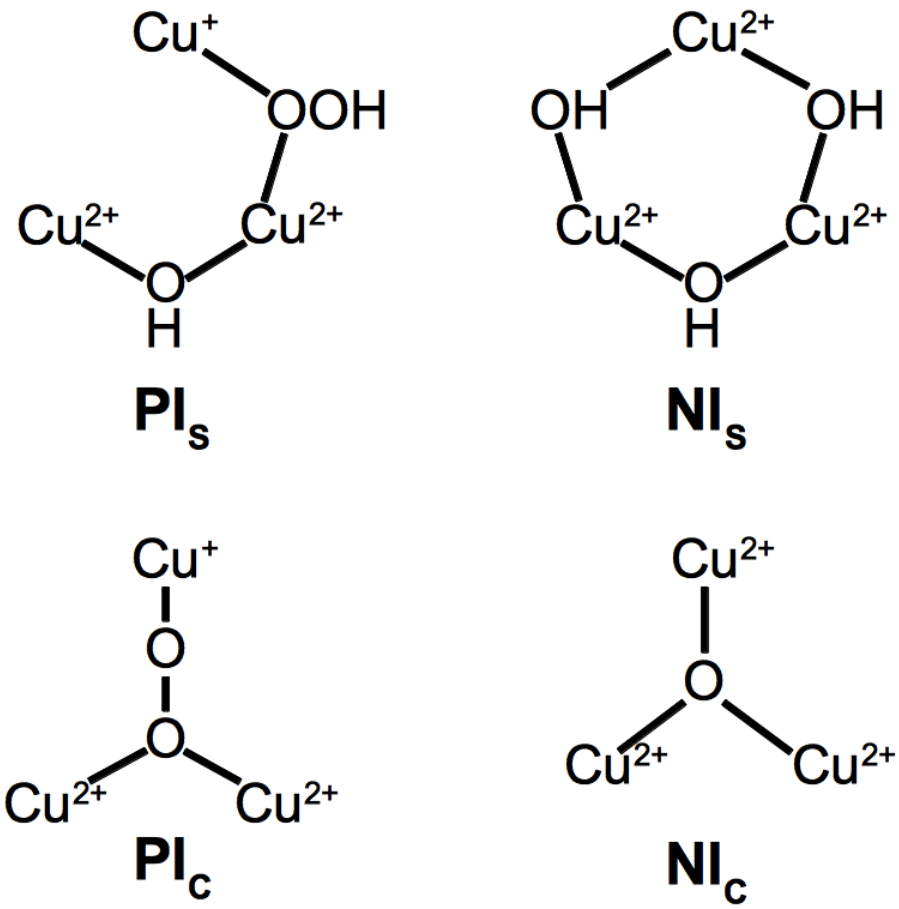

Figure 2: The two structural interpretations for the peroxy intermediate (**PI**) and the native intermediate (**NI**) suggested by Solomon from spectroscopic studies [15,35]. The subscripts distinguish the two binding modes (**S** with the ligand on the side, **C** with the ligand in the centre of the TNC).

Ox **Red** **PI**

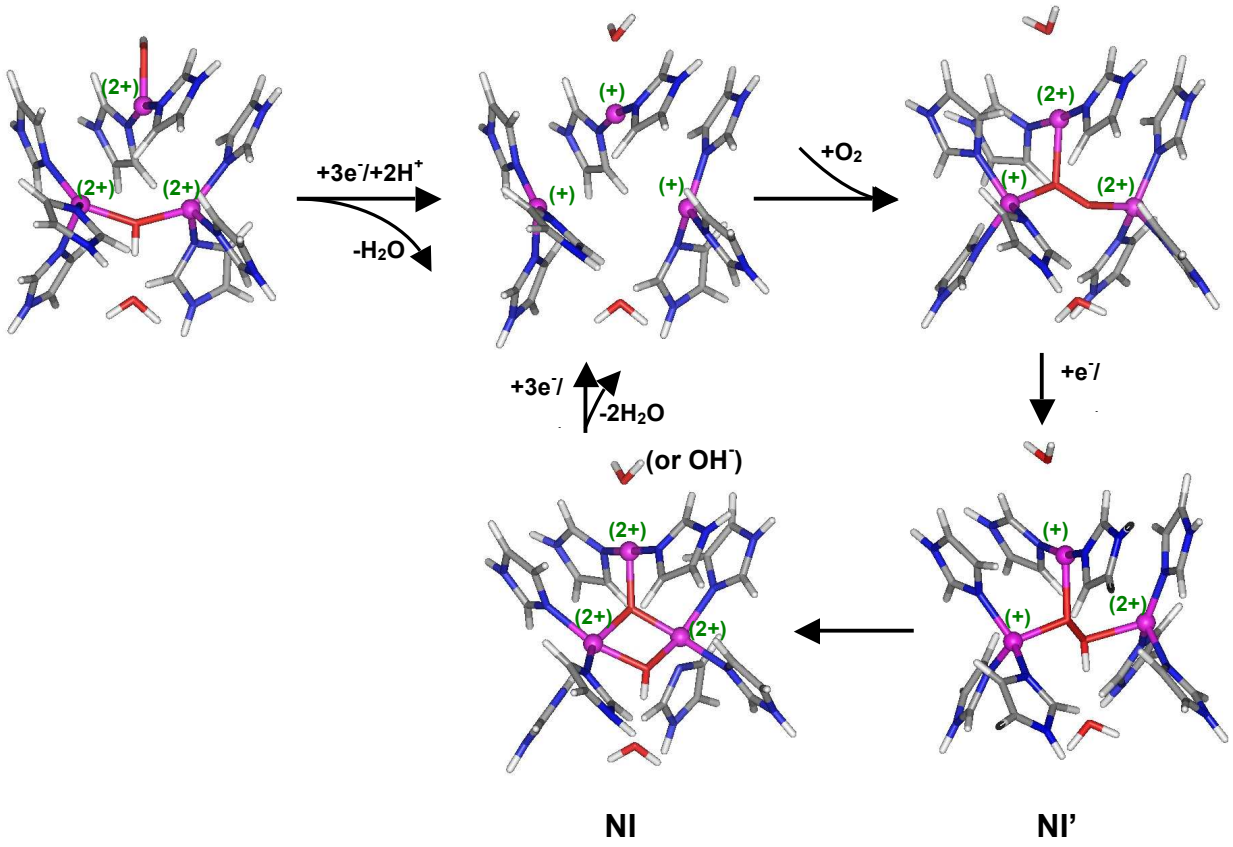

Figure 3: The Consensus Reaction Mechanism of the MCOs [9,13, 43]. Structural candidates for the oxidised resting state (**Ox**), the reduced state (**Red**), the peroxy intermediate (**PI**), the activated peroxy intermediate (**NI'**), and the native intermediate (**NI**) are depicted together with the flow of electron and protons in the cycle.

The results indicated that the resting **Ox** state of the protein has hydroxide ions both as the Cu-T2 ligand and as the bridging group between the two Cu-T3 ions, whereas the **Red** state was devoid of any bridging ligand but has a water ligand coordinated to the Cu-T2, which is in accordance with the experimental observations [44, 45,46]. For the **PI**, we obtained structures corresponding to the two possible candidates schematically drawn in Figure 2 (and also depicted in Figure 4), but the calculations predicted the structure with O_2^{2-} in the centre of the cluster (**PI**$_C$) to be the more likely candidate, since it is energetically much more favourable than the structure with HO_2^- bridging Cu-T2 one of the two Cu-T3 ions (**PI**$_S$). The reason for this is that there is simply too little space for a bridging ligand between

Cu-T2 and Cu-T3 and the flexibility of this region is rather limited owing to the four His–X–His links. The apical coordination of peroxide to one of the Cu-T3 ions observed in the crystal structure of ascorbate oxidase [44] could not be obtained in any of our geometry optimisations [13]. Last but not least, the calculated spin densities on the Cu-T2 and Cu-T3 ions (cf. Table 4 in Ref. [13]) were in qualitative agreement with the observed oxidation states of these ions (Cu-T2 and one of the Cu-T3 ions are oxidised) [41].

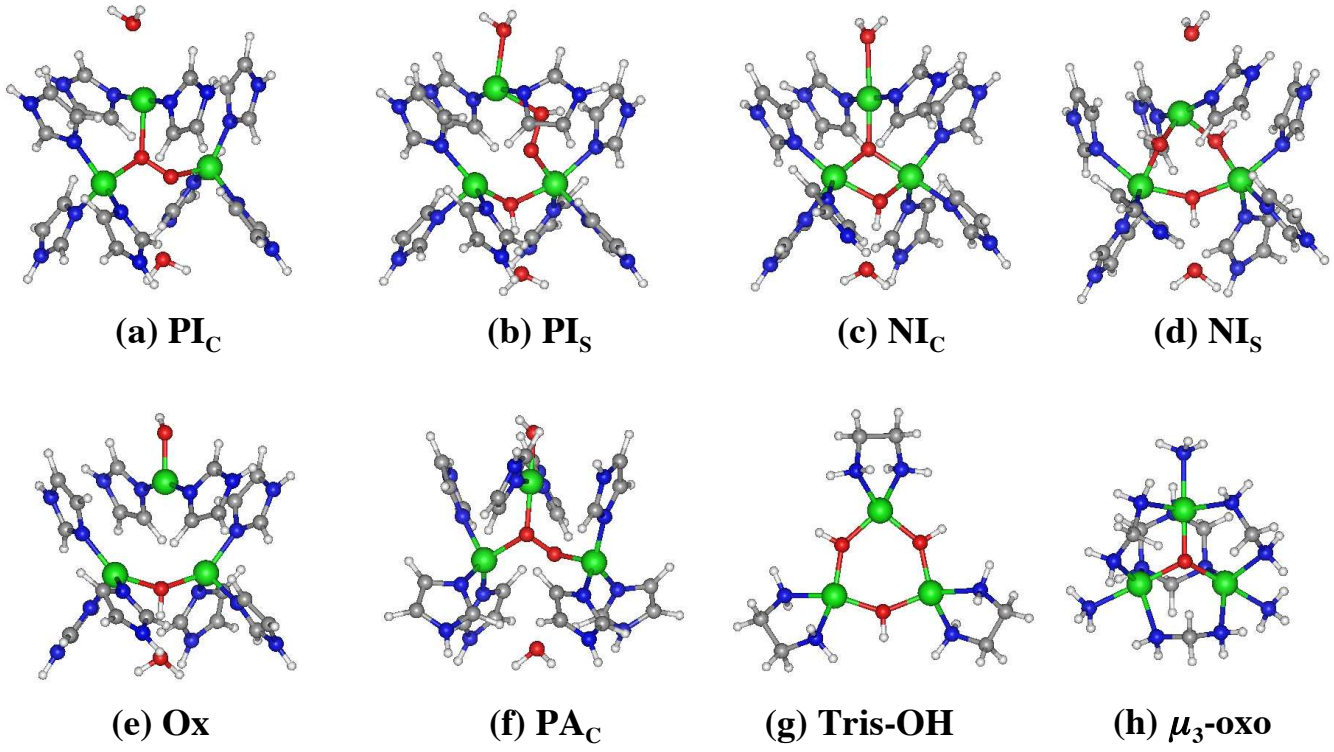

Figure 4: QM/MM models of the various MCO states (a) **PI$_C$**, (b) **PI$_S$**, (c) **NI$_C$**, (d) **NI$_S$**, (e) **Ox**, (f) **PA$_C$**, as well as QM-optimised structures of two inorganic models of the NI (g) **Tris-OH** and (h) **μ_3-oxo** (see the text for the definition of the used symbols).

Likewise, for the **NI**, the QM/MM results showed that the structure with an O^{2-} in the centre of the cluster (**NI$_C$**) is energetically more favourable than the structure with three OH^- ions bridging each of the pair of Cu ions (**NI$_S$**; both structures are shown in Figure 4). Again, this result is mainly owing to

the lack of space between the Cu-T2 and Cu-T3 ions; both structures yield similar geometries and electronic structures. Moreover, the $\mathbf{NI_C}$ structure also derives naturally in the reaction mechanism as the immediate product of the cleavage of the O–O bond in the **NI'** intermediate, formed by a one-electron reduction of the $\mathbf{PI_C}$ state.

Finally, it can be mentioned that in the interpretation of QM/MM results, it is important to take into consideration the accuracy of the theoretical method used. Our experience from the modelling of active sites of other copper proteins shows that the present method should give Cu–N and Cu–Cu distances that are accurate to within 0.07 and 0.12 Å, respectively [47,48]. The stiff bonds to the negatively charged O ligands are probably even more accurate (to within ~0.04 Å), whereas the positions of water molecules are determined by a delicate balance between the weak Cu–O interaction and possible hydrogen bonds to the surrounding protein and are therefore far from reliable. Considering that the average error in crystal structures with a resolution of 1.3–2.6 Å is ~0.1 Å and that errors of over 0.3 Å are frequently found [49,50], the QM/MM structures should be more accurate than the available medium-resolution crystal structures for the Cu coordination geometry.

In summary, the large-scale QM/MM calculations carried out for a large number of structural variants of the spectroscopically defined states in the MCO reaction cycle, complemented by their energetic stability, led to the first consistent picture of the MCO reaction mechanism (Figure 3) [13].

3.2. Ground-State Multiplicities and Excited States of the MCO Intermediates. DFT vs. Multi-Reference Wave Function Calculations. After formulating a consistent and plausible mechanism for the catalytic action of the MCOs [13], which was later confirmed experimentally [40], there still remained several details to be resolved. One of them was the incorrect ground-state multiplicity of the preferred $\mathbf{PI_C}$ model ($S = 1$) as predicted by the standard QM(DFT)/MM methods. As the assignment of the multiplicity of the ground electronic state and the prediction of accurate energy gaps between the various spin states can be a problem for DFT methods [51], multi-reference wave function calculations (specifically, multi-state second-order perturbation theory on a complete active-state self-consistent

field – MS-CASPT2/CASSCF and multi-reference difference dedicated configuration interaction – MRDDCI2 methods) were carried out [52]. The analysis of the ground- and excited-state energetics serves as a direct link between theory and experiment (i.e. the spectroscopic parameters obtained for these intermediates). The structures studied are depicted in Figure 4, besides that ammonia was used instead of the imidazole ligands.

In order to verify that the model systems and the *in vacuo* calculations of the spectroscopic parameters represent a valid model for correlating these data with experimental parameters obtained for the entire protein, we first made a simple and qualitative test. We studied three models of decreasing sophistication: a larger model including a point-charge model of the surrounding protein (the electrostatic effects; the mechanical effect was included explicitly since the structures were taken from the QM/MM optimised geometries) and imidazoles as more realistic models of the histidine residues, the same model without the point charges, and the smaller models with ammonia ligands that were used for the multi-reference calculations. At the DFT level, it was shown that the differences between the high-spin and low-spin splittings calculated for the three levels of description were only 0–9 $kJ.mol^{-1}$. This suggests that the smaller models of the studied intermediates can be used for excited-state calculations and the results can be correlated with the experimental data obtained for the MCO intermediates.

Using the MS-CASPT2/CASSCF calculations we were able to reproduce the experimentally observed low-spin ground states for all of the MCO intermediates, as well as a low-lying (~150 cm^{-1}) doublet state and a doublet–quartet energy gap of ~780 cm^{-1} for the **NI** [15]. The zero-field splitting (~70 cm^{-1}) of the ground state in a symmetric hydroxy-bridged trinuclear Cu(II) model of $\mathbf{NI_S}$ (**Tris-OH** in Figure 4) [53] was also quantitatively reproduced and a quantitatively correct quartet–doublet splitting (164 cm^{-1}) for the $\boldsymbol{\mu_3}$**–oxo**-bridged trinuclear Cu(II) model of $\mathbf{NI_C}$ was obtained (also in Figure 4) [40]. These results supported the suggestion that the $\mathbf{NI_C}$ and $\mathbf{PI_C}$ structures best reproduce the spectroscopic results, in agreement with the QM/MM results and the spectroscopic measurements based on the analysis of the pseudo A-term in the variable-temperature, variable-field MCD spectra [40].

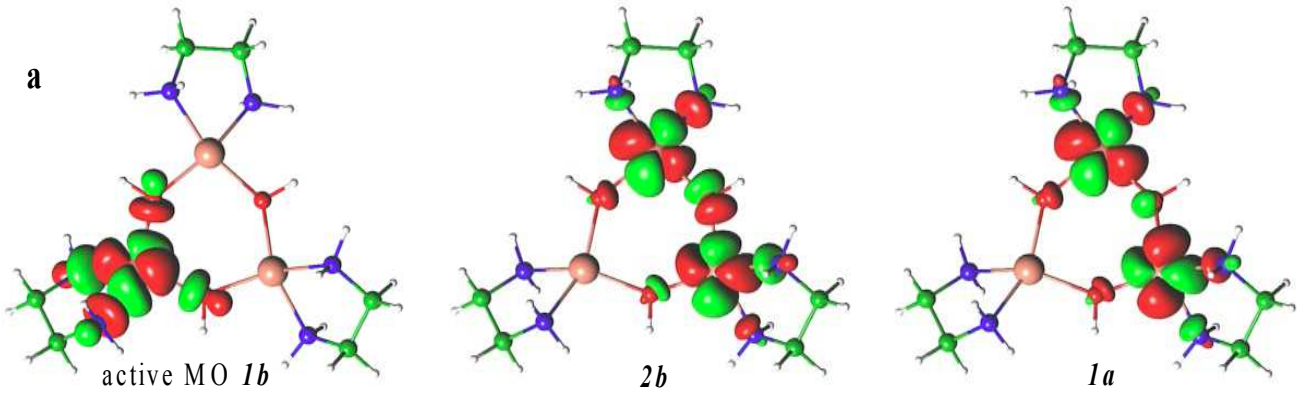

$1^2A\ (D_1) \sim 0.61((1a)^{\alpha}(1b)^2 - (1a)^{\alpha}(2b)^2) + 0.43(1a)^{\alpha}(1b)^{\beta}(2b)^{\alpha} - 0.25(1a)^{\alpha}(1b)^{\alpha}(2b)^{\beta}$

$1^2B\ (D_2) \sim 0.68((1a)^2(1b)^{\alpha} + (1b)^{\alpha}(2b)^2) + 0.20((1b)^2(2b)^{\alpha} - (1a)^2(2b)^{\alpha})$

$1^4A\ (Q_1) \sim 1.00(1a)^{\alpha}(1b)^{\alpha}(2b)^{\alpha}$

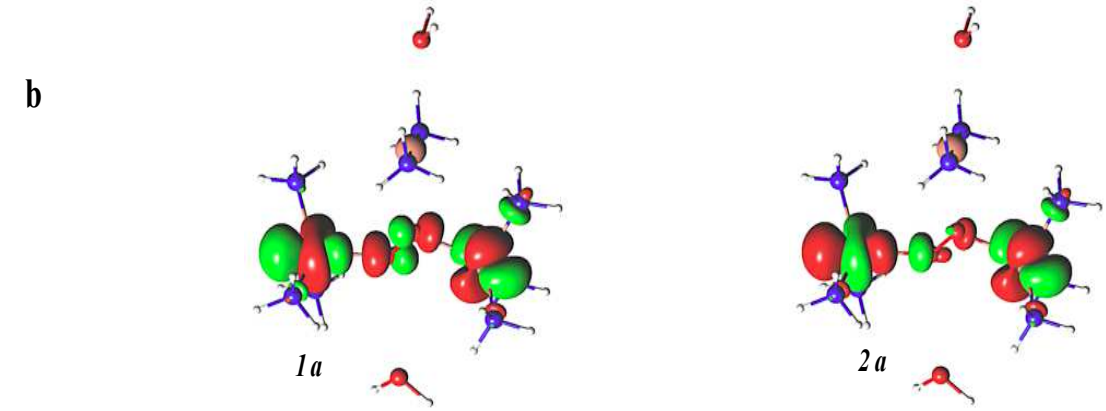

$1^1A\,(S_0) \sim 0.72(2a)^2 - 0.69(1a)^2$

$1^3A\,(T_1) \sim 1.00(1a)^{\alpha}(2a)^{\alpha}$

Figure 5: The three partially occupied active orbitals in the **Tris-OH** complex and the two partially occupied active orbitals for the $\mathbf{PI_C}$ model, together with the CI expansion coefficients. The two doublet and one quartet electronic states for **Tris-OH** originate from linear combinations of these orbitals. The same holds true for the lowest singlet and triplet state of the **PI**. The $N^{2S+1}X$ terms used in the figure denote the *N*th state of a symmetry X and $(2S + 1)$ spin multiplicity.

It can be concluded that the multi-reference wave function calculations carried out at optimised QM(DFT)/MM geometries represent a powerful tool to quantitatively predict low-lying excited states of the MCO intermediates and that the results can be directly correlated with the experimental spectroscopic results bringing another piece of information into the evolving picture of the overall reaction mechanism. As can be seen in Figure 5, an analysis of the active orbitals and the composition of the multi-reference wave function provide us also with a deep insight into the electronic structure of the TNC.

It should be mentioned that there have been recent attempts [54] to calculate the spin exchange between weakly interacting electron spins on different metal centres by introducing a new method based on spin-flip constricted variational density functional theory (SF-CV-DFT). It has been applied to predict the exchange coupling constants for the μ_3**–oxo** and **Tris-OH** models. It was concluded that the BHandHLYP DFT functional yielded the best fit to experiments and to the results of high-level calculations [52, 55] and that it can therefore probably be recommended for studies focusing on the spin-state energetics of the MCOs as a cheaper alternative to CASPT2.

3.3. Theoretical Calculations of the MCD Spectra of Trinuclear Copper Cluster Models. Recently, Ziegler and coworkers have developed and applied a computational scheme for the calculations of MCD spectra (including intensities of the transitions) employing a time-dependent (TD) DFT formalism. The developments included methods to calculate all three terms: the A- [56] and B-terms [57], as well as the temperature-dependent C-term [58]. The equations were developed for open-shell molecules and included spin-orbit coupling in the low- and high-temperature limits. The temperature-dependent MCD originates from two effects, viz. the breaking of degeneracy and the perturbation of transition dipoles by spin–orbit coupling. Having the theory at hand, the MCOs and their inorganic models represent both challenging and relevant systems to benchmark the methodology. To this end, the μ_3**–oxo** model was selected and the calculated TD-DFT MCD spectra included the zero-field splitting [59]. The simulated spectra nicely reproduced the shape and intensities of experimental spectra whereas the agreement of the

position of the peaks was satisfactory, although not perfect, as can be expected from the TD-DFT calculations on these electronically complex systems. Nevertheless, the study represents a significant step forward towards the understanding and interpretation of the MCD spectra of the MCOs, since the theoretical assignments are based on a direct first-principles simulations and may thus serve as the basis for a detailed molecular-orbital (MO) analysis. In this particular study, some details of the MO analysis differed from those based on a qualitative analysis of the MOs [40].

3.4. A Comparison with the EXAFS Spectra: A Combined QM/MM/EXAFS Procedure.

Another important source of experimental information concerning the structure of the metal sites in proteins is EXAFS spectroscopy [60,61]. As mentioned above, it is known from EXAFS studies that the **PI** has a Cu–Cu distance of ~3.4 Å [35] and that the **NI** has at least two Cu–Cu distances of 3.3 Å [15]. Unfortunately, this information was not detailed enough to discriminate between the two alternative interpretations of the two MCO intermediates: For example, in the QM/MM calculations, both the $\mathbf{PI_C}$ and $\mathbf{PI_S}$ structures gave a Cu–Cu distance of 3.53–3.57 Å, in reasonable agreement with the EXAFS data.

However, the EXAFS spectrum includes much more information than only a few interatomic distances. The question arises how this information can be extracted. To solve this problem, a method was developed that combines EXAFS refinement with QM geometry optimisations [62]. The idea was to employ the QM calculations in the same way as MM calculations are used to supplement X-ray crystallographic refinements and NMR structure determinations, i.e. to provide chemical information to ensure that the bond lengths and angles are reasonable, even if the experimental data are not accurate enough for such atomistic details [63,64,65]. It is analogical to the methods developed previously to combine QM/MM calculations with X-ray refinement and NMR structure determinations [66,67,68,69]. In brief, a QM structure of the site of interest is used as a starting structure and the EXAFS scattering amplitudes and phase shifts are calculated using the standard methods. With these, one performs an

EXAFS fit of only the energy-shift parameter (E_0; i.e. without changing the structure). Thereby, a goodness-of-fit estimate of the current structure, e.g. χ^2, is obtained. By a slight modification of the structure, e.g. by altering one bond length, we can measure how χ^2 changes and thereby calculate numerical EXAFS forces. Such forces for all interesting atoms can then be added to the QM forces and a standard geometry optimisation can be performed, yielding a structure that is an ideal compromise between the EXAFS data and the QM calculations.

A complication is that the QM and EXAFS energies have different units, viz. energy units for QM, but a unit-less quality descriptor (χ^2) for EXAFS. Therefore, they are not directly comparable. This was solved the same way as in X-ray and NMR refinement [63,65] by introducing a weight factor (w_{EXAFS}):

$$E_{\mathrm{EXAFS/QM}} = E_{\mathrm{QM}} + w_{\mathrm{EXAFS}}\, E_{\mathrm{EXAFS}} \qquad (2).$$

Considering that the overall accuracy of the EXAFS geometries (~0.01 Å [60,61]) is better than that of QM calculations (~0.05 Å [69,70]), w_{EXAFS} is normally increased until the geometry reaches a state when χ^2 does not change. Calibration studies showed that this EXAFS/QM approach worked excellently and actually could improve the EXAFS structures of small inorganic complexes (i.e. decrease χ^2 as compared to what is obtained with a standard EXAFS fit), because it involves information of the location of all the atoms in the system (i.e. full multiple-scattering information), not only a number of bond lengths. It has been employed to interpret the structure of sitting-atop complexes in the metallation of porphyrins and for the oxygen-evolving complex in photosystem II [71,72].

In order to be applicable to the MCOs, the method was extended to QM/MM calculations, so that the whole protein could be included in the calculations [16]. To test and verify the new methodology, $\mathbf{PA_C}$ and $\mathbf{PA_S}$ were compared at six levels of theory: standard EXAFS fits (of E_0 only) for the QM and QM/MM structures, EXAFS fits of the three Cu–Cu distances for the QM and QM/MM structures, as well as the combined EXAFS/QM and EXAFS/QM/MM methods. In all cases except one (the raw

QM/MM structure), the calculations indicated that the $\mathbf{PA_C}$ structure fitted the EXAFS data substantially better than the $\mathbf{PA_S}$ structure, as can be seen in Figure 6. This is confirmed by the χ^2 values, which are lower for $\mathbf{PA_C}$ than for the $\mathbf{PA_S}$ structure, 38 compared to 74. The structures remain close to the original QM/MM structures, with changes of less than 10 kJ.mol^{-1} in energy terms. This shows that QM/MM calculations can be used together with the EXAFS data to obtain more detailed structural information, and to interpret the EXAFS spectra and confirm that $\mathbf{PI_C}$ and $\mathbf{PA_C}$ are the most plausible structures. The true power of these combined schemes lies in the reconciliation of the computed (QM or QM/MM) data with the primary experimental data, and we are of the opinion that their full potential has not been yet fully exploited. Especially in the world of metalloproteins with many metal oxidation and ligand protonation states available, we consider them as the natural link between the experimental and theoretical domains.

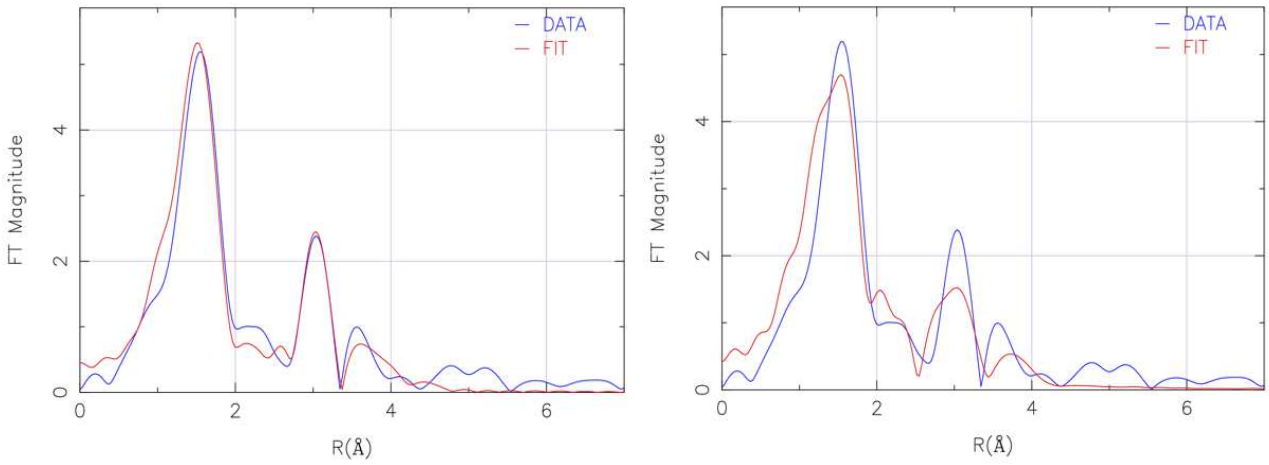

Figure 6: Comparison of the EXAFS data of the **PA** (blue traces) compared to the EXAFS spectrum obtained for the EXAFS/QM/MM calculations (red traces) for $\mathbf{PA_C}$ (left) and $\mathbf{PA_S}$ (right).

3.5. A Comparison with EPR Spectra: g Tensors of the MCO Intermediates. Nowadays, computational chemistry serves as a complementary tool to assist in the structural interpretation of observed EPR spectra. While the performance of quantum chemical methods for many organic radicals

is quite satisfactory, quantitative calculations of **g** tensors and hyperfine coupling constants (**A** matrix) for open-shell transition-metal systems are still challenging. Thanks to recent implementations of Neese [73] and Pierloot and Vancoillie [74], it is now possible to carry out these calculations using multi-reference wave function methods (CASSCF and MRCI), which provide a more rigorous alternative to DFT approaches in **g** tensor calculations. Using several notoriously problematic complexes – ($[Cu(NH_3)_4]^{2+}$, $[CuCl_4]^{2-}$ and $[Cu(imidazole)_2(CH_3SCH_3)(CH_3S)]^+$ – requiring a balanced treatment of all types of excited states, Vancoillie and Pierloot [75] showed that the MS-CASPT2 method can reproduce *g* values within 30 ppt. In particular, this approach was superior to the cheaper DFT(ZORA) calculations.

However, coupled three-spin systems, such as the TNC in MCOs, are even more challenging for the theory. As a natural step towards the calculation of EPR **g** tensors for the spin-frustrated TNC in MCOs, the methods were benchmarked on a conceptually simpler system: Cu^{2+} hexafluoroacetylacetonate with two pyrazole-substituted nitronyl nitroxides ($Cu(hfac)_2L^R$) [55]. This system is a member of a family of heterospin polymer-chain complexes [76], the so-called breathing crystals, and exhibits structural rearrangements at low temperatures, giving rise to magnetic anomalies in the temperature dependence of the effective magnetic moment, similar to a classical spin crossover. Calculated *g* factors obtained using CASSCF/CASPT2 (with an active space of 13 electrons in 13 orbitals), $g_{\|} = 1.848$, $g_{\perp} = 1.965, 1.974$ were in agreement with the experimentally observed $g < 2$ signals in the low-temperature EPR spectra [55].

Encouraged by this finding, we turned our attention to the MCOs and small inorganic MCO models [77]. Again, the key issues were to identify the correct structures of the **NI**, **PI** and **Ox** states and to obtain a correlation between the spectroscopic and calculated data, which would provide further evidence for the proposed reaction mechanism. Instead of EPR-silent **PI**, we considered its EPR-active, one-electron-oxidised **PA** analogue, which exhibits similar spectroscopic characteristics and is likely to have a similar structure.

For the **Tris-OH** complex, the calculations yielded equatorial $g_{x,y}$ factors close to zero for all four methods used (CASSCF, CASPT2, MS-CASPT2 and MRCI-S) in agreement with the expected $g_{\perp} = 0$ value (which cannot be measured directly, but was obtained from the spin Hamiltonian) for a symmetric **Tris-OH** structure [53]. The experimental value of $g_{\parallel} = 2.32$ [53] was reproduced only qualitatively; the best calculated values were 2.46–2.49. The overestimation of $g_{\parallel}$ was analogous to what Vancoillie and Pierloot found for the mononuclear copper complexes [75]. However, the reasonable agreement obtained enabled us to analyse the contributions of the ground and excited states to the overall *g* value. It has been convincingly shown [77] that the main contributions arise from the ground state and the first excited ligand-field state, confirming an earlier orbital-based analysis of Yoon and Solomon [53].

The $\mathbf{NI_C}$ and $\mathbf{NI_S}$ structures do not possess a trigonal symmetry and therefore the EPR pattern arises from the two doublet states and one quartet state, which all are possible candidates for the ground state. The calculations of the EPR **g** tensors were highly non-trivial and the two methods (CASPT2 and MRCI-S) gave results that differed considerably. One source of the discrepancy is the high sensitivity of the *g* factors to the energy gap between the two low-lying doublet states, which strongly influences the values of g_1 and g_2 (and to a lesser extent the largest g_3 value). The MRCI-S results for both **NI** structures were closer to the experimental values [15] but the observed discrepancies (both between experiment and calculations and between the two methods) precluded an unambiguous structural assignment. Nevertheless, the unusual $g < 2$ factors were qualitatively reproduced and it was proved that both structures are indeed consistent with the experimental EPR data.

Finally, in the resting **Ox** state, a normal Cu-T2 EPR signal was reported experimentally ($g_x = 2.04$, $g_y = 2.05$, $g_z = 2.24$) [46]. Using MS-CASPT2, $g_1 = 2.07$, $g_2 = 2.09$ and $g_3 = 2.53$ were obtained. Keeping in mind a systematic overestimation of the $g_{\parallel}$ values, as was observed also for the **Tris-OH** and **NI** systems, the agreement between the MS-CASPT2 results and the experiment is reasonable and qualitatively correct. Contrary to what was observed for the **NI**, the MRCI-S method underestimated the *g* factors.

In summary, multi-reference wave function methods yielded qualitatively correct and sometimes even semiquantitative results for the EPR **g** tensors for these complicated three-spin systems, in contrast to

standard DFT methods, which failed to do so. This can be instrumental also in interpreting the results of related systems of great interest, e.g. trinuclear copper pyrolato frameworks [78]. However, even with a great level of diligence and expertise, this might not be enough to provide an unambiguous structural interpretation but may rather serve as an independent proof of the overall consistency of the selected structural models.

4. Dioxygen Cleavage by MCOs: The Reaction Mechanism

The central part of the overall enzymatic action in the MCOs is the cleavage of the O–O bond of O_2. This reaction takes place in the TNC and starts when the TNC is in the **Red** state. When O_2 binds to TNC in the **Red** state, it is instantaneously reduced by two electrons to the peroxide level, forming the **PI**. It is then assumed that the **PI** takes up one electron from Cu-T1, forming a transient species, **NI'** (sometimes denoted as **PI +e**). This is the state that immediately precedes the O–O bond cleavage, resulting in the formation of the **NI**. The key structures in the reaction cycle are depicted in Figure 3.

It has been described in the previous sections how computational chemistry assisted in the elucidation of the candidates for the various intermediates in the reaction cycle. What remained to be characterised was the reaction coordinate for the actual O–O bond cleavage.

The first theoretical calculations of the pathways for the cleavage of the O–O bond and characterisation of the transition-state barriers were carried out by Yoon and Solomon on cluster models of the TNC [79]. They obtained transition-state barriers of 23-25 kJ.mol^{-1} for the proton-assisted and proton-unassisted pathways (i.e. with the peroxide moiety protonated and deprotonated; the Cu-T2 ligand was H_2O) and the overall reaction was shown to be highly exothermic, by ~213 kJ.mol^{-1}, which originates from the high exothermicity (ΔH) of the uncatalysed $H_2 + H_2O_2 \rightarrow 2\ H_2O$ reaction (ΔH = – 347 kJ.mol^{-1}) [80]. However, owing to the complicated structure of the MCO active site, it is unclear whether a QM cluster model may yield reliable results.

Therefore, the QM/MM method has been used to study six pathways differing in the protonation of the peroxide ligand (O_2^{2-} or HO_2^- bound to **NI'**) and the nature of the ligand coordinated to the Cu-

T2 ion (water, OH^-, or none) [43]. Besides finding the structures of transition states and computing the activation (free) energy, the question addressed in the study was whether O_2^{2-} is protonated prior to the O–O bond cleavage. The results of the calculations are compiled in Table 2.

Table 2: Calculated QM/MM activation barriers ($\Delta G^{\neq}_{QM/MM}$) and reaction energies ($\Delta G_{QM/MM}$) for the O–O bond cleavage in CueO. The data are compiled from Tables 1, 2, and 3 in Ref. [43]. The geometries were optimised at the QM(RI-PBE/DZP)/MM level, whereas single-point energies were recalculated at the QM(B3LYP/def2-TZVP)/MM level. The thermal and entropic contributions were calculated from frequency calculations on the corresponding cluster models and the range of values for $\Delta G^{\neq}_{QM/MM}$ corresponds to two methods of approximate optimisations of transition states at the QM/MM level. All of the values are in $kJ.mol^{-1}$.

Cu-T2 ligand	Central ligand	Charge of QM Region	$\Delta H^{\neq}_{therm} - T\Delta S^{\neq}$	$\Delta G^{\neq}_{QM/MM}$	$\Delta H_{therm} - T\Delta S$	$\Delta G_{QM/MM}$
H_2O	O_2H^-	+1	-2.5	67	15	-43
OH^-	O_2H^-	0	-	–	13	-88
–	O_2H^-	+1	-1.2	74-79	18	-8
H_2O	O_2^{2-}	0	1.3	71-72	13	52
OH^-	O_2^{2-}	-1	5.6	64-67	23	-79
–	O_2^{2-}	0	4.5	77-78	16	52

It can be seen from the data in Table 2 that we obtained activation barriers for all of the six pathways that are qualitatively consistent with the experimental rate constant of $k > 350\ s^{-1}$ [81] (corresponding to a barrier of ~60 $kJ.mol^{-1}$ using the Eyring equation). Moreover, the overall exothermicity decreased significantly using QM/MM calculations. Based solely on the QM/MM calculations, we may rule out two pathways that are endergonic. Furthermore, the higher exergonicity (-80 and -90 $kJ.mol^{-1}$) might disfavour another two pathways and therefore, one may hypothesise that

the most conceivable pathway is the one with the H_2O as the Cu-T2 ligand and the peroxide moiety protonated, and conclude that the protonation of the **NI'** intermediate occurs prior to the cleavage of the O–O bond. However, the other pathway without protonation (OH^-:O_2^{2-}; analogous to the proton-unassisted pathway described by Yoon and Solomon [79]) has almost identical barrier is also feasible, although the exergonicity is much higher.

In summary, the QM/MM calculations complemented previous QM calculations [79] and have provided somewhat more realistic reaction energetics. The calculations have verified the overall plausibility of the consensus reaction mechanism and provided some further details.

5. Electron-Transfer Properties of the MCOs

Above, we have described how QM and QM/MM calculations have provided useful information to understand the part of the reaction mechanism of the MCOs for which experimental data are available, i.e. the **Ox**, **Red**, **PI** and **NI** states. However, the reaction cycle also involves the reduction of the **NI** to the **Red** state and therefore, at least two additional formal oxidation levels of the TNC - $(Cu^+)(Cu^{2+})_2$ and $(Cu^+)_2(Cu^{2+})$ – come into play (denoted as the **IOx** and **IRed** states). This reduction consists of three steps of one-electron transfer from Cu-T1 to the TNC. Concomitantly, the two oxygen species in the **NI** (two O^{2-} or O^{2-} + OH^-) should be protonated and dissociate prior to the next catalytic cycle. Depending on the order of these reduction and protonation steps, a number of different intermediates can be imagined.

The experimental information on the mutual perturbation of Cu-T1 site and the TNC is rather scarce. Augustine *et al.* [82] have investigated the influence of the mutation of the two His Cu-T3 ligands that lie along the Cu-T1 → Cu-T23 ET pathway to Gln and Cys residues. By using resonance Raman spectroscopy, they showed that these mutations increase the covalency of the Cu–S bond at the Cu-T1 site and decrease the Cu-T1 reduction potential by up to 75 mV. This study, together with the lack of other extensive experimental data highlights the necessity of theoretical calculations that can be used to

study these reactions. QM/MM structures can easily be obtained for all of the conceivable intermediates. However, it is much more difficult to obtain reliable estimates of the reaction energies, because electron- and proton-transfer steps are involved. This implies that the net charge of the active sites changes, which makes it difficult to obtain converged energies. On the other hand, if reliable reduction potentials and pK_a values of the TNC could be obtained, the most probable reaction sequence for the reduction of the **NI** could be established. In this section, we will describe the computational efforts directed towards this aim.

5.1 Reorganisation Energies. According to the semiempirical Marcus theory, the rate of electron transfer can be estimated from the equation:

$$k_{ET} = \frac{2\pi}{\hbar} \frac{\left|H_{DA}\right|^2}{\sqrt{4\pi\lambda k_B T}} \exp(-\frac{(\Delta G + \lambda)^2}{4\lambda k_B T}) \qquad (3)$$

where ΔG is the driving force of the reaction (i.e. the difference in the redox potential), H_{DA} is the electronic coupling between the donor and the acceptor, and λ is the reorganisation energy. The latter is the energy required to relax the structure and environment upon electron transfer, i.e. the energy difference of the product state in its equilibrium geometry and in the equilibrium geometry of the reactant state, and vice versa. It is often divided into two parts, namely the inner-sphere reorganisation energy (λ_{is}), which comes from the redox site itself, and the outer-sphere reorganisation energy (λ_{os}), which comes from the surrounding protein and solvent. λ_{is} can be estimated by QM methods, employing the definition, e.g. by calculating the energy difference between the oxidised state in its equilibrium geometry and in the equilibrium geometry of the reduced state, and vice versa, using small cluster models of the redox-active site in the calculations (e.g. a metal ion and its first-sphere ligands) [83,84,85,86]. For a protein site, it is more accurate to use QM/MM methods to obtain the structures of the redox site, and it is typically observed that λ_{is} is lower when calculated in the protein than in vacuum

[85,87,88]. For example, λ_{is} for a QM model of an isolated Cu-T1 site is 62–88 kJ.mol^{-1} [84], whereas it is 30–50 kJ.mol^{-1} lower in proteins like plastocyanin and azurin [87].

However, estimating λ_{os} normally requires more complicated methods, based on molecular-dynamics (MD) simulations of a fully solvated protein. A common approach, originally suggested by Warshel [89], is based on Marcus parabolas and a linear-response approximation. Several other groups have developed extensions to this theory, as well as other methods to calculate λ at various levels of theory, including MM, QM/MM, and QM [88,90,91,92].

For the small Cu-T1 protein azurin, a total λ of 68–99 kJ.mol^{-1} has been measured for the electron transfer from the Cu site to a Ru label on the surface of the protein [93]. Moreover, the Cu-T1 sites have been studied with theoretical methods, yielding λ_{os} = 42–54 kJ.mol^{-1} for plastocyanin–cytochrome *f* complexes with docked geometries [94] and 70–90 kJ.mol^{-1} for the reduction of the Cu-T1 sites in four different MCOs from short (10 ps) QM/MM MD simulations [92].

We have studied the total λ for the electron transfer between the reduced Cu-T1 site and the TNC in the **PI** state in the CueO protein [95]. To this end, a tailored MM parameterisation of the Cu-T1 and TNC sites in the MCO (i.e. the two sites of highest interest) was constructed, employing the accurate method by Norrby and Liljefors [96], which allows for a nearly perfect reproduction of the metal-site geometry [97]. Then, a long MD simulation of the protein was performed. From the energy difference of the metal sites before and after the electron transfer, λ was calculated with the methods of Warshel, Sprik and Blumberger [88,89,90] both at the MM and QM/MM levels. The result was quite insensitive to the theoretical treatment (λ = 91–133 kJ.mol^{-1}). Moreover, the calculations allowed us to divide the total λ into various components. First, it can be divided into λ_{is} and λ_{os}. The former includes contributions from Cu-T1 and TNC, 12 and 22 kJ.mol^{-1}, respectively. This is appreciably lower than for the isolated QM clusters (57 and 61 kJ.mol^{-1}) and also slightly smaller than the corresponding QM/MM energies (15 and 30 kJ.mol^{-1}). Moreover, λ_{os} can be further divided into contributions from the bonds, angles, dihedrals, van der Waals interactions, and electrostatics, and the results show that it is completely dominated by electrostatics. Finally, λ_{os} can also be divided into contributions from the

solvent and from the various residues in the protein. It turns out that only 37% of λ_{os} comes from the solvent. The remainder comes from residues in the protein and many residues contribute to this energy – the two largest contributions are only 8 and 4 kJ.mol^{-1} and come from two residues close to the Cu-T1 site.

It was also shown that λ_{os} can be calculated from minimised QM/MM structures, which gave results that were typically 10–30 kJ.mol^{-1} lower than those from MD simulations, owing to a restricted relaxation of the surrounding protein and water. On the other hand, the QM/MM calculations are much faster and do not require a special parameterisation of the metal sites. Therefore, we have employed QM/MM calculations to estimate λ for two additional states in the MCO cycle, namely the **NI → IOx** and **IOx → IRed** transformations [98]. The results were 88–99 and 91–108 kJ.mol^{-1} for the two processes, respectively. This is quite similar to λ of the **PI → NI'** transition, indicating that there are no major differences between the various electron-transfer steps in the MCO reaction cycle.

In summary, theoretical calculations have shown that the reorganisation energies for the MCO are ~100 kJ.mol^{-1} for all three electron-transfer steps studied which is similar to what is found for other electron-transfer proteins. The calculations also allow a division of this energy into components from the metal sites, as well as from the residues in the surrounding protein and from the solvent.

5.2 Reduction Potentials. Many methods to calculate the redox potentials of metal sites in proteins have been developed. A first estimate can be obtained by simply calculating the QM energies of the active-site clusters in a continuum solvent. However, to obtain information on the influence of the surrounding protein, more sophisticated methods are needed [88,90,99,100,101,102,103,104]. Many groups have estimated and rationalised the redox potentials of Cu-T1 proteins [102,105,106,107,108,109,110]. The main problem with the calculation of absolute redox potentials is that it involves a change of the net charge of the studied system. This leads to very large electrostatic energies and long-range solvation effects [104,111]. For example, the Coulombic interaction between

two groups with a unit charge is 93 kJ.mol^{-1} (0.96 V) at 15 Å (although it is probably screened by a dielectric constant of 4–80) and the Born solvation energy in water of a unit charge is 23 kJ.mol^{-1} (0.24 V) even for a spherical system of a 30-Å radius. This makes the calculation of the absolute redox potentials a formidable task.

For the MCOs, one can exploit the fact that the electron transfer to the TNC proceeds via the Cu-T1 site. It is therefore sufficient to study this internal electron transfer between the Cu-T1 and the TNC, which involves a transport of an electron by ~13 Å but it does not change the net charge of the simulated system. Therefore, the calculated energies are expected to be more stable. Moreover, the reduction potential of the Cu-T1 site is experimentally known for many enzymes [92] and therefore the absolute redox potential of the TNC can be deduced from the calculated difference in the reduction potentials of the two sites.

In fact, we can calculate the energy difference for the **PI**–Cu^{+}-T1 → **NI'**–Cu^{2+}-T1 electron-transfer reaction from the simulations used to calculate λ, discussed in the previous section [88,90,95], which measures the difference in the redox potential between the reduced Cu-T1 site and the **PI** state of the TNC. The result was 87 kJ.mol^{-1} (0.91 V) in favour of the oxidised Cu-T1 site and the **NI'** state [95]. Again, the energies can be decomposed into the contributions of the QM sites (0.43 and 4.7 V for the Cu-T1 and TNC sites, respectively; these estimates are large, because solvation effects are missing) and from the surrounding protein (325 kJ.mol^{-1}). The latter comes entirely from electrostatic interactions. Moreover, it comes almost completely from the surrounding water – the net protein effect is only 4 kJ.mol^{-1}. However, this is only a coincident as there are numerous large contributions from protein residues, up to 131 kJ.mol^{-1} for charged groups close to the two copper sites, but they happen to cancel completely in this case.

Unfortunately, the calculated relative redox potentials are sensitive to details in the theoretical treatment (owing to the transfer of a unit charge by ~13 Å). We have calculated the same difference in the redox potentials with several other methods [95]. For example, the redox potential difference

decreases by 20 kJ.mol^{-1} if it is calculated by electrostatic embedding rather than mechanical embedding in the QM/MM calculations (i.e. if the electrostatic interactions between the QM and MM systems are calculated by QM rather than by MM). A similar change was observed if the DFT method was varied, whereas the basis-set effects are ~10 kJ.mol^{-1}. If isolated models of the two Cu sites in a dielectric continuum are used, energy differences of 28–154 kJ.mol^{-1} can be obtained depending on the dielectric constant of the continuum (4–80), showing that such an approach is very unreliable. Standard QM/MM calculations provide an energy difference of ~40 kJ.mol^{-1} with electrostatic embedding but 72–106 kJ.mol^{-1} with mechanical embedding. When these were supplemented with a continuum solvation model of the solvent surrounding the protein using the QM/MM-PBSA approach [112] (with mechanical embedding), the energy was somewhat stabilised at 111–120 kJ.mol^{-1}.

Finally, we tried also QM/MM free-energy perturbations using the QTCP (QM/MM thermodynamic cycle perturbation) approach [113]. It allows for full flexibility of the protein, except that the two Cu sites are fixed at the QM/MM structures. Interestingly, it yielded an energy difference of ~45 kJ.mol^{-1}. Approximately 10 kJ.mol^{-1} of the difference between the QTCP and MD results comes from differences in the treatment of the long-range electrostatic effects (i.e. solvation outside the ~55 Å radius of the explicitly simulated system; the MD simulations use particle-mesh Ewald summation, whereas the QTCP calculations use the Onsager relation). The rest comes from differences in the geometries in the sampled snapshots. This may indicate that the MM force field of the Cu centres is not accurate enough to extract reliable QM energy differences. On the other hand, the Cu sites have fixed geometries in the QTCP calculations, which is also a somewhat questionable approximation. This shows that it is hard to calculate relative redox potentials to an accuracy better than ~25 kJ.mol^{-1} (0.3 V). On the other hand, it is likely that the differences in the reduction potentials between various states of the TNC site are more accurate.

Using the QM/MM-PBSA method, we can estimate how the two Cu clusters in MCOs interact with each other. Clearly, it is completely meaningless to discuss the redox potential of the TNC without specifying the state of the cluster (**Ox**, **Red**, **PI**, **NI**, **IOx** or **IRed**), because these states have quite

varying reduction potentials, which also strongly depend on the protonation states of the Cu ligands. It seems more reasonable to discuss the redox potential of the Cu-T1 site, because it has only two different states. However, the two Cu clusters are separated by only 13 Å, so it is likely that the state of one cluster will affect the redox potential of the other (the Coulomb interaction between two unit charges at this distance is 25 $kJ.mol^{-1}$ (0.25 V) assuming a dielectric constant of 4). Our preliminary QM/MM-PBSA calculations [114] indicate that the potential of the TNC increases by 0.05–0.09 V if the Cu-T1 is oxidised. Conversely, the redox potential of the Cu-T1 may vary by up to 0.38 V as an effect of the redox and protonation state of the TNC, as can be seen in Figure 7. This larger effect is caused by the larger net charge of the TNC and the larger variation in the oxidation and protonation states: We have tested 38 different models with a net charge of the TNC Cu ions and the first-sphere ligands from +1 to +5. However, it is likely that many of these states never arise in the protein, owing to their unfavourable redox potentials or pK_a values. Still, it is clear that there is significant communication between the two redox sites in MCOs. These results are in accordance with the experimental observation that the redox potentials of Cu-T1 changes by up to 75 mV when two His ligands of the TNC were mutated [82].

In summary, the results show that it is hard to calculate accurate reduction potentials and that the reduction potentials of Cu-T1 and the TNC in the MCOs are coupled to each other.

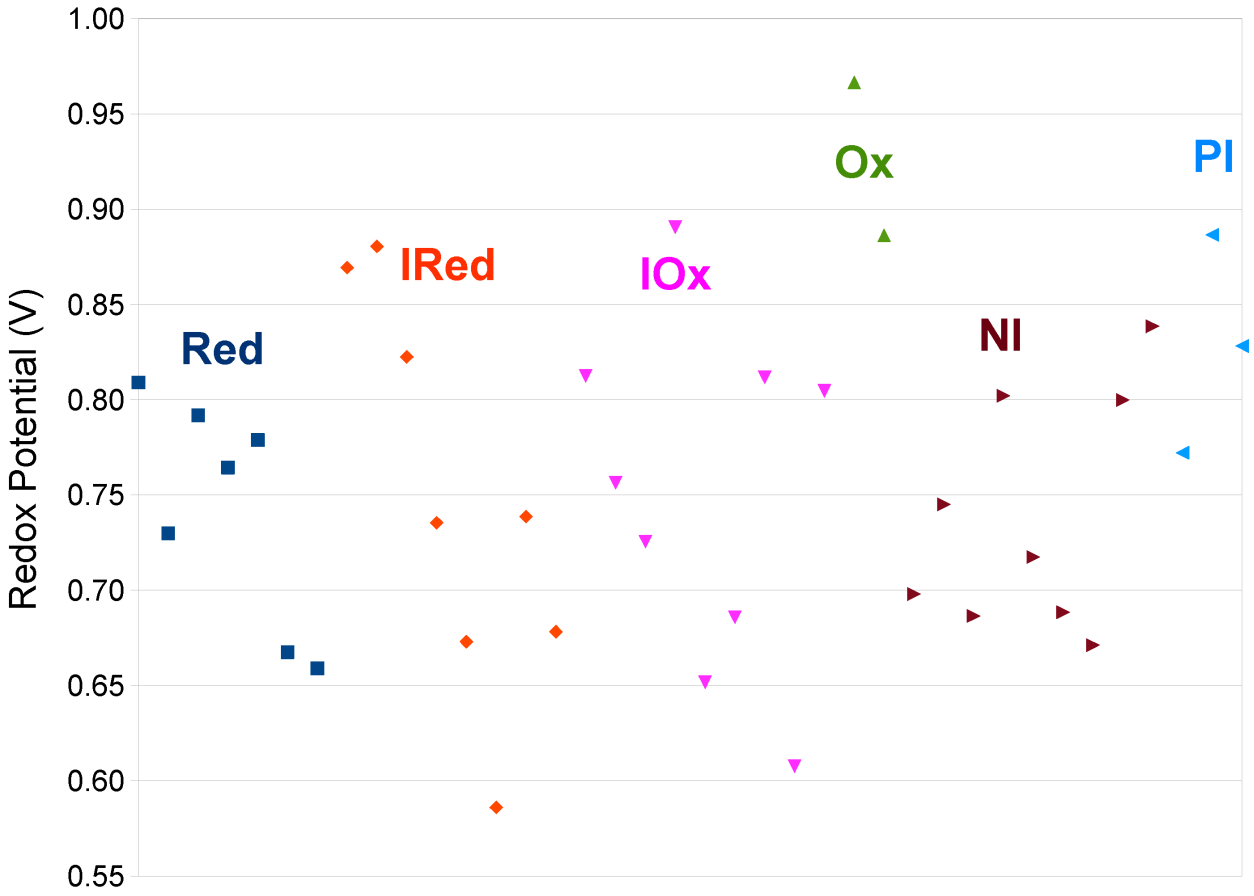

Figure 7. Variation of the Cu-T1 redox potential when the oxidation and protonation state of the TNC is varied according to QM/MM-PBSA calculations [114]. The redox potential has been calculated for 38 possible states of the TNC. They are grouped according to the oxidation state of the TNC (**Red**, **IRed**, **IOx**, **NI**, and **PI**), as indicated, and the various calculations within each group differ in the protonation states of the solvent or O_2-derived ligands. For example, the two calculations for the **Ox** state differs in whether the Cu-T2 ligand is H_2O or OH^-.

5.3 The Full Reaction Mechanism. What remains in order to obtain a complete picture of the intermediates of the MCO reaction mechanism is to determine the acidity constants (pK_a values) of the various states. These can be estimated with similar computational methods as were used for the redox

potentials [100,101,104,115]. These reactions involve a change in the net charge of the simulated system, which makes the calculations sensitive to the treatment of long-range electrostatics and boundary conditions [111], but in this case, it is less evident how it can be solved by some sort of internal proton transfer, even though it is conceivable to let a group on the protein surface or a molecule in solution be the proton acceptor. We have preliminary QM/MM-PBSA results for most conceivable intermediates in the reaction mechanism [114], which are in good accordance with the available experimental data, e.g. that the two water-derived Cu ligands in the **Ox** state both are OH^- ions [46]. As for the redox potentials, the results show that the pK_a values of the TNC are reduced by 0.5–2.0 pK_a units if the Cu-T1 site is oxidised. Combining the calculated pK_a values and redox potentials, we can suggest a complete reaction cycle of MCOs, which is shown in Figure 8. We are currently working on the corresponding more accurate QTCP results for all of these reactions.

Figure 8. Suggested reaction mechanism of the MCOs, including all intermediates [114], even in the **NI** → **Red** pathway. The formal oxidation states of individual copper ions are not depicted since these are not always uniquely determined from the calculations due to the delocalization of the electrons.

6. Concluding Remarks

In this tribute to the impressive work of Prof. Edward Solomon in the field of multicopper oxidases, we have reviewed recent theoretical contributions that have been essential to our understanding of the structure and function of this class of enzymes. Starting with a survey of the experimental X-ray crystal structures and discussing the caveats in the local structural details caused by the partial reduction of copper ions in the TNC that influence the interatomic distances, we demonstrated how QM(DFT)/MM calculations elucidated the structures of the experimentally defined intermediates. The complicated electronic structure of the TNC makes it hard to obtain quantitatively correct spectroscopic data from

the DFT methods. Therefore, multi-reference wave function methods (e.g. CASPT2 and MRCI-S) need to be used to obtain quantitative splitting of the lowest doublet and quartet states, reliable excitation energies of ligand-field states, and qualitatively correct predictions of the **g** tensors for these spin-frustrated systems. The quest for the verification of the theoretical data resulted in the development and application of combined EXAFS/QM/MM schemes that couple EXAFS fitting with QM and QM/MM geometry optimisation. Finally, the intramolecular electron transfer between the Cu-T1 site and the TNC has been studied using QM/MM MD and QTCP methods to obtain reliable reorganisation energies and correlate them with the experimental rate constants. Finally, ongoing efforts to achieve an understanding of the full mechanism involving calculations of the reduction potentials and the acidity constants of the reaction intermediates are mentioned. In most of the described studies, Ed Solomon was an active collaborator and it has been a privilege for the authors to work with him.

References

[1] A. Messerschmidt, In *Multicopper oxidases*; Messerschmidt, A., Ed.; World Scientific: Singapore; River Edge, NJ, 1997; pp. 23-80.

[2] E.I. Solomon, U.M. Sundaram and T.E. Machonkin, Chem. Rev. 96 (1996) 2563.

[3] L. Quintanar, C.S. Stoj, A.B. Taylor, P.J. Hart, D.J. Kosman, E.I. Solomon, Acc. Chem. Res. 40 (2007) 445.

[4] D.J. Spira-Solomon, M.D.Allendorf, E.I. Solomon, J. Am. Chem. Soc. 1986, 108, 5318.

[5] A. Messerschmidt, R. Ladenstein, R. Huber, M. Bolognesi, L. Avigliano, R. Petruzzelli, A. Rossi, A. Finazzi-Agro, J. Mol. Biol. 224 (1992) 179.

[6] E.I. Solomon, P. Chen, M. Metz, S.-K. Lee, A.E. Palmer, Angew. Chem. Int. Ed. 40 (2001) 4570.

[7] I. Bento, M.A. Carrondo, P.F. Lindley, J. Biol. Inorg. Chem. 11 (2006) 539.

[8] J. Yoon, E.I. Solomon, Coord. Chem. Rev. 251 (2007) 379.

[9] E.I. Solomon, A.J. Augustine, J. Yoon, Dalton Trans. (2008) 3921.

[10] E.I. Solomon, J.W. Ginsbach, D.E. Heppner, M.T. Kieber-Emmons, C.H. Kjaergaard, P.J. Smeets, L. Tian, J.S Woertink, Faraday Discuss 148 (2011) 11.

[11] I. Bento, L.O. Martins, G.G. Lopes, M.A. Carrondo, P.F. Lindley, Dalton Trans. (2005) 3507.

[12] S.A. Roberts, A. Weichsel, G. Grass, K. Thakali, J.T. Hazzard, G. Tollin, C. Rensing, W.R. Montfort, Proc. Natl. Acad. Sci. U.S.A. 99 (2002) 2766.

[13] L. Rulíšek, E.I. Solomon, U. Ryde, Inorg. Chem. 44 (2005) 5612.

[14] A.J. Augustine, L. Quintanar, C.S. Stoj, D.J. Kosman, E.I. Solomon, J. Am. Chem. Soc. 129 (2007) 13118.

[15] S.-K. Lee, S. D. George, W. E. Antholine, B. Hedman, K. O. Hodgson, E. I. Solomon, J. Am. Chem. Soc. 124 (2002) 6180-6193.

[16] U. Ryde, Y.-W. Hsiao, L. Rulíšek, E. I. Solomon, J. Am. Chem. Soc. (2007) 129, 726-727.

[17] K. Piontek, M. Antorini, T. Choinowski, J. Biol. Chem. 277 (2002) 37663.

[18] N. Hakulinen, L.L. Kiiskinen, K. Kruus, M. Saloheimo, A. Paananen, A. Koivula, J. Rouvinen, Nat. Struct. Biol. 9 (2002) 601.

[19] M. Ferraroni, N.M. Myasoedova, V. Schmatchenko, A.A. Leontievsky, L.A. Golovleva, A. Scozzafava, F. Briganti, BMC Struct. Biol. 7 (2007) 60.

[20] N. Hakulinen, M. Andberg, J. Kallio, A. Koivula, K. Kruus, J. Rouvinen, J. Struct. Biol. 162 (2008) 29.

[21] J.P. Kallio, S. Auer, J. Jänis, M. Andberg, K. Kruus, J. Rouvinen, a Koivula, N. Hakulinen, J. Mol. Biol. 392 (2009) 895.

[22] P. Durão, Z. Chen, C.S. Silva, C.M. Soares, M.M. Pereira, S. Todorovic, P. Hildebrandt, I. Bento, P.F. Lindley, L.O. Martins, Biochem. J. 412 (2008) 339.

[23] T.J. Lawton, L.A. Sayavedra-Soto, D.J. Arp, A.C. Rosenzweig, J. Biol. Chem. 284 (2009) 10174.

[24] C.S. Silva, P. Durão, A. Fillat, P.F. Lindley, L.O. Martins, I. Bento, Metallomics 4 (2012) 37.

[25] I. Bento, C.S. Silva, Z. Chen, L.O. Martins, P.F. Lindley, C.M. Soares, BMC Struct. Biol. 10 (2010) 28.

[26] H. Komori, K. Miyazaki, Y. Higuchi, FEBS Lett. 583 (2009) 1189.

[27] X. Li, Z. Wei, M. Zhang, X. Peng, G. Yu, M. Teng, W. Gong, Biochem. Biophys. Res. Commun. 354 (2007) 21.

[28] J.P. Kallio, J. Rouvinen, K. Kruus, N. Hakulinen, Biochemistry 50 (2011) 4396.

[29] S. Garavaglia, M.T. Cambria, M. Miglio, S. Ragusa, V. Iacobazzi, F. Palmieri, C. D'Ambrosio, A. Scaloni, M. Rizzi, J. Mol. Biol. 342 (2004) 1519.

[30] A.V. Lyashenko, N.E. Zhukhlistova, A.G. Gabdoulkhakov, Y.N. Zhukova, W. Voelter, V.N. Zaitsev, I. Bento, E.V. Stepanova, G.S. Kachalova, O.V. Koroleva, E. a Cherkashyn, V.I. Tishkov, V.S. Lamzin, K. Schirwitz, E.Y. Morgunova, C. Betzel, P.F. Lindley, A.M. Mikhailov, Acta Crystallogr. F-Struct. Biol. Cryst. Commun. 62 (2006) 954.

[31] T. Bertrand, C. Jolivalt, P. Briozzo, E. Caminade, N. Joly, C. Madzak, C. Mougin, Biochemistry 41 (2002) 7325.

[32] F.J. Enguita, L.O. Martins, A.O. Henriques, M.A. Carrondo, J. Biol. Chem. 278 (2003) 19416.

[33] S.A. Roberts, G.F. Wildner, G. Grass, A. Weichsel, A. Ambrus, C. Rensing, W.R. Montfort, J. Biol. Chem. 278 (2003) 31958.

[34] M.-E. Zaballa, L. Ziegler, D.J. Kosman, A.J. Vila, Journal of the American Chemical Society 132 (2010) 11191.

[35] W. Shin, U.M. Sundaram, J.L. Cole, H.H. Zhang, B. Hedman, K.O. Hodgson, E.I. Solomon J. Am. Chem. Soc. 118 (1996) 3202.

[36] J. Yoon, B.D. Liboiron, R. Sarangi, K.O. Hodgson, B. Hedman, E.I. Solomon, Proc. Natl. Acad. Sci. U. S. A. 104 (2007) 13609.

[37] L.B. LaCroix, S.E. Shadle, Y. Wang, B.A. Averill, B. Hedman, K.O. Hodgson, E.I. Solomon, J. Am. Chem. Soc. 118 (1996) 7755.

[38] K. Pierloot, J.O.A. De Kerpel, U. Ryde, M.H.M. Olsson, B.O. Roos, J. Am. Chem. Soc. 120 (1998) 13156.

[39] D.J. Spira-Solomon, E.I. Solomon, J. Am. Chem. Soc. 109 (1987) 6421.

[40] J. Yoon, L.M. Mirica, T.D.P. Stack, E.I. Solomon, J. Am. Chem. Soc. 127 (2005) 13680.

[41] A.J. Augustine, C. Kjaergaard, M. Qayyum, L. Ziegler, D.J. Kosman, K.O. Hodgson, B. Hedman, E.I. Solomon, J. Am. Chem. Soc. 132 (2010) 6057.

[42] U.M. Sundaram, H.H. Zhang, B. Hedman, K.O. Hodgson, E.I. Solomon, J. Am. Chem. Soc. 119 (1997) 12525.

[43] M. Srnec, U. Ryde, L. Rulíšek, Faraday Discuss. 148 (2011) 41.

[44] A. Messerschmidt, H. Luecke, R. Huber, J. Mol. Biol. 230 (1993) 997.

[45] A.E. Palmer, L. Quintanar, S. Severance, T.-P. Wang, D.J. Kosman, E.I. Solomon, Biochemistry 41 (2002) 6438.

[46] L. Quintanar, J. Yoon, C.P. Aznar, A.E. Palmer, K.K. Andersson, R.D. Britt, E.I. Solomon J. Am. Chem. Soc. 127 (2005) 13832.

[47] M.H.M. Olsson, U. Ryde, J. Am. Chem. Soc. 123 (2001) 7866.

[48] U. Ryde, M.H.M. Olsson, Int. J. Quantum Chem. 81 (2001) 335.

[49] U. Ryde, K. Nilsson, J. Mol. Struct. (THEOCHEM) 632 (2003) 259.

[50] U. Ryde, K. Nilsson, J. Am. Chem. Soc. 125 (2003) 14232.

[51] M. Reiher, Inorg. Chem. 41 (2002) 6928.

[52] J. Chalupský, F. Neese, E.I. Solomon, U. Ryde, L. Rulíšek, Inorg. Chem. 45 (2006) 11051.

[53] J. Yoon, L.M. Mirica, T.D.P. Stack, E.I. Solomon, J. Am. Chem. Soc. 126 (2004) 12586.

[54] H. Zhekova, M. Seth, T. Ziegler, J. Chem. Theor. Comput. 7 (2011) 1858.

[55] S. Vancoillie, L. Rulíšek, F. Neese, K. Pierloot, J. Phys. Chem. A 113 (2009) 6149.

[56] M. Seth, M. Krykunov, T. Ziegler, J. Autschbach, J. Chem. Phys. 128 (2008) 234102

[57] M. Seth, J. Autschbach, T. Ziegler, J. Chem. Theor. Comput. 3 (2007) 434.

[58] M. Seth, T. Ziegler, J. Autschbach, J. Chem. Phys. 129 (2008) 104105.

[59] H.R. Zhekova, M. Seth, T. Ziegler, J. Phys. Chem. A 115 (2011) 10323.

[60] J.M. Charnock, Radiat. Phys. Chem. 45 (1995) 358.

[61] J.E. Penner-Hahn, Coord. Chem. Rev. 192 (1999) 1101.

[62] Y.-W. Hsiao, Y. Tao, J.E. Shokes, R.A. Scott, U. Ryde Phys. Rev. B, 74 (2006) 214101.

[63] G.J. Kleywegt, T.A. Jones, Methods Enzymol. 227 (1997) 208.

[64] G.J. Kleywegt, T.A. Jones, Acta Crystallogr. Sect. D-Biol. Crystallogr. 54 (1998) 1119.

[65] J. Cavanagh, W.J. Fairbrother, A.G. Palmer, N.J. Skelton Protein NMR Spectroscopy. Principles and Practice (1996), Academic Press, London.

[66] U. Ryde, L. Olsen, K. Nilsson, J. Comput. Chem. 23 (2002) 1058.

[67] U. Ryde, K. Nilsson, J. Am. Chem. Soc. 125 (2003) 14232.

[68] Y.-W. Hsiao, T. Drakenberg, U. Ryde, J. Biomol. NMR 31 (2005) 97.

[69] U. Ryde, Dalton Trans. (2007) 607.

[70] F. Neese, J. Biol. Inorg. Chem. 11 (2006) 702.

[71] Y.-W. Hsiao, U. Ryde, Inorg. Chim. Acta 359 (2005) 1081.

[72] X. Li, E.M. Sproviero, U. Ryde, P.E.M. Siegbahn, V.S. Batista, G. Chen, Int. J. Quantum Chem. (2012), submitted.

[73] F. Neese, Chem. Phys. Lett. 380 (2003) 721.

[74] S. Vancoillie, P.-Å. Malmqvist, K. Pierloot, ChemPhysChem 8 (2007) 1803.

[75] S. Vancoillie, K. Pierloot, J. Phys. Chem. A 112 (2008) 4011.

[76] S.L. Veber, M.V. Fedin, A.I. Potapov, K.Y. Maryunina, G.V. Romanenko, R.Z. Sagdeev, V.I. Ovcharenko, D. Goldfarb, E.G. Bagryanskaya, J. Am. Chem. Soc. 130 (2008) 2444.

[77] S. Vancoillie, J. Chalupský, U. Ryde, E.I. Solomon, K. Pierloot, F. Neese, L. Rulíšek, J. Phys. Chem. B 114 (2010) 7692.

[78] G. Mezei, R.G. Raptis, J. Telser, Inorg. Chem. 45 (2006) 8841.

[79] J. Yoon, E.I. Solomon, J. Am. Chem. Soc. 129 (2007) 13127.

[80] P.W. Atkins, Physical Chemistry (1978) Oxford University Press, Oxford, U. K.

[81] A.E. Palmer, S.-K. Lee, E.I. Solomon, J. Am. Chem. Soc. 123 (2001) 123 6591.

[82] A.J. Augustine, M.E. Kragh, R. Sarangi, S. Fujii, B.D. Liboiron, C.S. Stoj, D.J. Kosman, K.O. Hodgson, B. Hedman, E.I. Solomon, Biochemistry 47 (2008) 2036.

[83] A. Klimkans, S. Larsson, Chem. Phys. 189 (1994) 25.

[84] M.H.M. Olsson, U. Ryde, B.O. Roos, Protein Sci. 7 (1998) 2659.

[85] E. Sigfridsson, M.H.M Olsson, U. Ryde, Inorg. Chem. 40 (2001) 2509.

[86] E. Sigfridsson, M.H.M. Olsson, U. Ryde, J. Phys. Chem. B 105 (2001) 5546.

[87] U. Ryde, M.H.M. Olsson, Int. J. Quantum Chem. 81 (2001) 335.

[88] J. Blumberger, Phys. Chem. Chem. Phys. 10 (2008) 5651.

[89] A. Warshel, J. Phys. Chem. 86 (1982) 2218.

[90] Y. Tateyama, J. Blumberger, M. Sprik, I. Tavernelli, J. Chem. Phys. 122 (2005) 234505.

[91] X. Zeng, H. Hu, X. Hu, A.J. Cohen, W. Yang, J. Chem. Phys. 128 (2008) 124510.

[92] G. Hong, D.M. Ivnitski, G.R. Johnson, P. Atanassov, R. Pachter, J. Am. Chem. Soc. 133 (2011) 4802.

[93] J.R. Winkler, P. Wittung-Stafshede, J. Leckner, B.G. Malmström, H.B. Gray, Proc. Natl. Acad. Sci. U. S. A. 94 (1997) 4246.

[94] G.M. Soriano, W.A. Cramer, L.I. Krishtalik, Biophys. J. 73 (1997) 3265.

[95] L. Hu, M. Farrokhnia, J. Heimdal, S. Shleev, L. Rulíšek, U. Ryde, J. Phys. Chem. B 115 (2011) 13111.

[96] P.-O. Norrby, T. Liljefors, J. Comput. Chem. 19 (1998) 1146.

[97] L. Hu, U. Ryde J. Chem. Theory Comput. 7 (2011) 2452.

[98] S. Shleev, C. Reimann, V. Andoralov, M. Falk, T. Ruzgas, M. Srnec, U. Ryde, L. Rulíšek, Electroanalysis (2012), submitted.

[99] A. Warshel, W.W. Parson, Annu. Rev. Phys. Chem. 42 (1991) 279.

[100] G.M. Ullmann, E.-W. Knapp, Eur. Biophys. J. 28 (1999) 533.

[101] L. Noodleman, W.-G. Han, J. Biol. Inorg. Chem. 11 (2006) 674.

[102] M.H.M. Olsson, G. Hong, A. Warshel, J. Am. Chem. Soc. 125 (2003) 5025.

[103] M. Sulpizi, S. Raugei, J. VandeVondele, P. Carloni, M. Sprik, J. Phys. Chem. B 111 (2007) 3969.

[104] J. Heimdal, M. Kaukonen, M. Srnec, L. Rulíšek, U. Ryde, ChemPhysChem. 12 (2011) 3337.

[105] S.N. Datta, J. Sudhamsu, A. Pandey, J. Phys. Chem. B 108 (2004) 8007.

[106] M. Cascella, A. Magistrato, I. Tavernelli, P. Carloni, U. Rothlisberger, Proc. Natl. Acad. Sci. U. S. A. 103 (2006) 19641.

[107] M.L. Barrett, I. Harvey, M. Sundaraajan, R. Surendran, J.F. Hall, M.J. Ellis, M.A. Hough, R.W. Strange, I.H. Hillier, S.S. Hasnain, Biochemistry 45 (2006) 2927.

[108] K. Paraskevopoulos, M. Sundaraajan, R. Surendran, M.A. Hough, R.R. Eady, I.H. Hillier, S.S. Hasnain, Dalton Trans. (2006) 3067.

[109] D.N. LeBard, D.V. Matyushov, J. Phys. Chem. B 112 (2008) 5218.

[110] D. Si, H. Li, J. Phys. Chem. A 113 (2009) 12979.

[111] G. Hummer, L.R. Pratt, A.E. García, J. Phys. Chem. A 102 (1998) 7885.

[112] M. Kaukonen, P. Söderhjelm, J. Heimdal, U. Ryde, J. Phys. Chem. B 112 (2008) 12537.

[113] T.H. Rod, U. Ryde, Phys. Rev. Lett. 94 (2005) 138302.

[114] J. Li, M. Farrokhnia, L. Rulíšek, U. Ryde, manuscript in preparation.

[115] E. Alexov, E.L. Mehler, N. Baker, A.M. Baptista, Y. Huang, F. Milletti, J.E. Nielsen, D. Farrell, T. Carstensen, M.H.M. Olsson, J.K. Shen, J. Warwicker, S. Williams, J.M. Word, Proteins 79 (2011) 3260.